ELSEVIER

Polymer 43 (2002) 4791–4801

polymer

www.elsevier.com/locate/polymer

Compatibiliser activity and morphology stability during twin-screw extrusion and injection moulding of compatibilised blends

A. Tabtiang, R.A. Venables*

Department of Chemistry, Faculty of Science, Mahidol University, Rama VI Road, Bangkok 10400, Thailand

Received 5 December 2001; received in revised form 1 April 2002; accepted 18 April 2002

Abstract

The influence of screw speed, agitator configuration, and compatibiliser, namely maleated polypropylene (mPP), during twin-screw extrusion upon the morphology, dispersion stability, and properties of polyamide-6/polypropylene (PA6/iPP) blends has been investigated. For mPP contents of 2.4 vol% and greater, the number average domain diameters measured in the extruded compound, $D_{n(ex)}$, were found to decrease to a limiting value at the specific mechanical energy input, S_e, around 0.07 kW h kg^{-1}, when S_e was controlled by the screw configuration and screw speed. For mixing energies greater than 0.07 kW h kg^{-1}, the domain size was principally determined by the ratio of specific interfacial area, S_{ext}, between the PA and iPP phases to the estimated volume fraction of in situ formed copolymer, ϕ_c; $S_{ext}/\phi_c \approx 45\ \mu m^{-1}$. The difference, ΔD_n, between $D_{n(ex)}$ and the average domain diameter measured in the cores of the samples after injection moulding, $D_{n(m)}$, was calculated: $\Delta D_n = |D_{n(ext)} - D_{n(m)}|$. It was found that $\Delta D_n \propto D_{n(ext)}$; i.e. larger droplets in the extrudate underwent the greatest changes in dimension in the subsequent moulding process.

Keywords: Compatibiliser; Compounding; Injection moulding

1. Introduction

Immiscible blends may be compatibilised through the addition of block copolymers or reactive additives that lead to the in situ formation of interface active species [1]. Compatibilised blends of polyamides and polyolefins are of the latter type. Typically, a maleic anhydride (MA) grafted polyolefin is added to the blend leading to the reaction of the anhydride groups of the compatibiliser with amine end-groups of the polyamide. The in situ formed copolymer comprises polyolefin and polyamide blocks; high concentrations of anhydride may result in reaction of the amide groups in the backbone of the polyamide [2]. Gonzalez-Montiel et al. [3] showed that the dispersed domain size in polyamide-6 (PA6)/polypropylene (iPP)/polypropylene-*graft*-MA (mPP) blends decreased with increasing loading of mPP in the blend and with increasing anhydride content in the mPP. Moreover, it was reported that mPP materials that possessed, on average, greater than one anhydride functional group per iPP molecule gave rise to bimodal size distributions in the blends in which they were the compatibiliser. It was proposed that this observation was related either to the immiscibility of mPP with iPP, or to the formation of comb-shaped copolymers, and possibly micelles, that were less efficient compatibilisers than the mono-functional mPP samples that formed in situ di-block copolymers. For polyamides possessing amine groups at both ends of the polymer chain, reaction with MA-grafted polymers led to the formation of looped or cross-linked structures that gave rise to complex composite dispersed phase morphologies [4]. The incompatibility of the polyamide block with the polyolefin phase, and the incompatibility of the polyolefin block with the polyamide phase, results in its preferential location at the polyolefin/polyamide interface [5]. This was found to lead to the formation of a 40 nm thick interphase in amorphous (aPA)/mPP 7/3 w/w blends, in comparison with a value of 4.8 nm for the corresponding aPA/iPP blend. The coil dimensions of the iPP block in the in situ formed compatibiliser, described by the radius of gyration, was estimated to be 10 nm. It was inferred that the thick interphase comprised multiple layers of in situ formed compatibiliser that prevented coarsening of the morphology during static annealing in the melt-state. Jannerfeldt [6] described a deformed drop-retraction procedure from which it was found that the addition of 30 wt% mPP, containing 0.3 wt% of MA, reduced the interfacial tension between iPP and PA6

* Corresponding author. Tel.: +662-2461-358; fax: +662-2458-332.
E-mail address: frrav@mahidol.ac.th (R.A. Venables).

0032-3861/01/$ - see front matter
PII: S0032-3861(02)00289-6

Table 1
Physical characteristics at the extrusion conditions of 230 °C and 1.4 MPa of the base resins and the PA6/iPP blend, containing 60 vol%, of PA

Property	Symbol	PA	mPP	iPP	Blend
Melt flow index	MFI (dg min^{-1})	–	110[a]	10[a]	–
Molecular weight	M (g mol^{-1})	21 000[b]	97 500[c]	264 000[c]	–
Reactive functionality	$[x]_0$ (μmol g^{-1})	49.1[d]	45.9[e]	0	–
Specific heat capacity	C_P (J g^{-1} K^{-1})	2.70[f]	1.95[g]	1.95[g]	–
Thermal conductivity	κ (W m^{-1} K^{-1})	0.21[h]	0.16[h]	0.16[h]	–
Thermal diffusivity	α (cm^2 s^{-1})	0.09[i]	0.11[j]	0.11[j]	0.10[k]
Heat of fusion	ΔH_f (kJ kg^{-1})	130[l]	100[l]	100[l]	–
Specific volume	V_s (cm^3 g^{-1})	1.17[m]	1.34[m]	1.34[m]	1.22[k]
Molar volume	V_m (cm^3 mol^{-1})	113.7[n]	56.4[n]	56.4[n]	–
Density	ρ (g cm^{-3})	0.855[o]	0.746[o]	0.746[o]	0.817[k]

[a] BS 720A test condition 12.
[b] Number average molecular weight from amine end-group titration.
[c] Weight average molecular weight from GPC analysis [4].
[d] Amine end-groups $[NH_2]_0$.
[e] Anhydride groups $[A]_0$ [31].
[f] Ref. [10].
[g] Calculated from $C_P = \kappa/\rho\alpha$.
[h] Ref. [11].
[i] Calculated from $\alpha = \kappa/\rho C_P$.
[j] Ref. [12].
[k] Calculated from the weight fraction weighted averages of the values for PA and iPP.
[l] Ref. [13].
[m] Ref. [14].
[n] Calculated from $V_m = V_s M_0$, where M_0 is the molecular weight of the polymer repeat unit.
[o] Calculated from $V = \rho^{-1}$.

from around 12.5 mN m^{-1} in its absence to approximately 5 mN m^{-1} in its presence at 225 °C. Moreover, the domain sizes observed in twin-screw extruded melt blends after quenching in water were related to the experimentally determined interfacial tension. However, Kirjava et al. [7] reported a value for the PA6/iPP interfacial tension of 7.8 mN m^{-1} at 250 °C, determined through the imbedded fibre retraction method and a value of 13.3 mN m^{-1} at 250 °C calculated from the harmonic mean of the surface tension of PA6 and iPP found in the literature. Additionally, Asthana [8] reported the interfacial tension of the PA6/iPP interface as 10 mN m^{-1} determined through the fitting of a mathematical model of the melt properties of an emulsion to rheological data obtained at 230 °C. Apparently, there is considerable variation between the various experimental interfacial tension values. Sundararaj and Macosko [9] showed that the most important influence of compatibilisers is to arrest coalescence and that the reduction in interfacial tension that enhanced dispersive mixing was of much less importance.

The objectives of this work were to extend the previous studies [5,6] to an investigation of the interactions between twin-screw extrusion conditions, namely screw configuration and screw speed, and compatibiliser activity in the range of realistic conditions of flow history found during melt processing. In addition, the relationship between initial morphology produced in the twin-screw extruder and its stability under typical injection moulding is presented. The PA6/iPP/mPP system was chosen since the in situ reaction has been characterised in previous work [2] and is of commercial importance [1].

2. Experimental

2.1. Materials

The resins used were PA6, grade 1013 NB from Thai Petrochemical Industry/Ube Co. Ltd, iPP homopolymer, grade P600F from Thai Polyethylene Co. Ltd, and the mPP grafted with 0.45 wt% MA was Fusabond 109D from Dupont Co. Ltd. Physical data for these materials are listed in Table 1.

2.2. Melt processing

Compounding was carried out using a Prism 16 mm diameter, fully intermeshing, co-rotating twin-screw extruder; all barrel temperature zones were set at 230 °C. The melt discharge temperatures were measured using a probe thermocouple inserted into the melt. The feed hopper was operated at a constant, arbitrary, screw speed; the consequent gravimetric output rate, Q_g, was determined, to an accuracy of ± 0.1 g min^{-1}, for each extrusion run; e.g. for run #1, $Q_g = 1.80$ kg h^{-1}. The blend ratio was 6/4, PA6/iPP, based upon volume, assuming densities of iPP and PA6 at 25 °C of 0.905 and 1.100 g cm^{-3}, respectively. The compounding conditions are given in Table 2. In the

Table 2
Compounding conditions and impact data

	Run #	Screw configuration	Screw speed (min^{-1})	mPP content[a] (vol%)	Impact energy[b]	
					Notched (kJ m^{-2})	Unnotched (kJ m^{-2})
	0	C	150	0.0	3.0 (0.1)	27.0 (1.6)
Factorial points	1	A	100	1.0	3.8 (0.9)	65.5 (17.0)
	2	B	100	1.0	3.7 (0.2)	76.5 (5.1)
	3	A	200	1.0	3.7 (0.2)	84.7 (7.6)
	4	B	200	1.0	3.0 (0.2)	54.4 (8.9)
	5	A	100	3.8	5.3 (0.5)	>98[c]
	6	B	100	3.8	6.3 (0.7)	>98[c]
	7	A	200	3.8	6.0 (1.0)	>98[c]
	8	B	200	3.8	6.3 (0.6)	>98[c]
Centre points	9	A	150	2.4	5.0 (0.3)	88.0 (10.5)
	10	B	150	2.4	6.6 (0.8)	>98[c]
	11	A	150	2.4	5.1 (0.2)	>98[c]
	12	B	150	2.4	5.2 (0.2)	>98[c]
Pure resins	PA6	–	–	–	3.7 (0.5)	>98[c]
	iPP	–	–	–	2.5 (0.5)	>98[c]

[a] Based upon densities at 25 °C for iPP and mPP of 0.905 g cm^{-3}; density for PA was 1.100 g cm^{-3}.
[b] Values in parenthesis are the sample standard deviations.
[c] Reported for specimens that were not broken with the largest Charpy impact striker.

formulations containing mPP, it was assumed that the density of mPP was 0.905 g cm^{-3} at 25 °C. The screws had a length to diameter, D, ratio of 25 to 1. For the compounding of the blends containing compatibiliser, the agitators were arranged into two configurations, denoted A and B, as illustrated in Fig. 1; the mixing paddles arrangements, i.e. 90°, F30°, and F60°, are defined in Fig. 2. Configuration A was designed to give relatively low energy dissipation with progressive melting in the range 1–18D. Configuration B was intended to confer high mechanical energy input; it contained a half reverse pitch screw at $D = 9.5$ after a 3D long section of mixing paddles in the range 7–9D. For the uncompatibilised blend, configuration C was used. Configuration C was essentially the same as B, except that in C the D/2 reverse screw was removed and a D/2 forwarding screw was added at a distance of 6D from the first screw element; i.e. before the first sequence of mixing paddles.

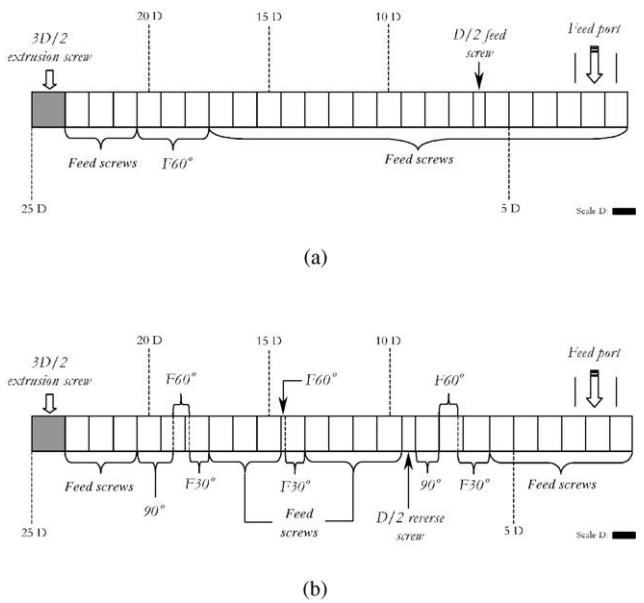

Fig. 1. Screw configuration A and B; the mixing paddles arrangements, i.e. 90°, F30°, and F60°, are defined in Fig. 2. The vertical scale is double the horizontal scale.

2.3. Testing

Mechanical test specimens were prepared with a 22-ton Boy injection-moulder, with a barrel and mould temperature of 230 and 80 °C, respectively. Screw speed was 100 min^{-1} and back pressure 0 MPa. The hopper was heated to 90 °C with a hot air blower to keep the feed stock dry. Specimens were stored in sealed tins containing silica gel desiccant for at least 1 week before testing dry, as moulded, at 25 °C and

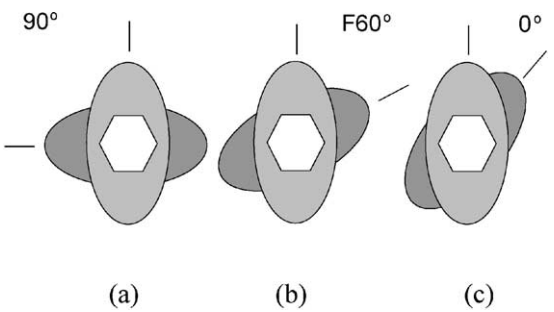

Fig. 2. Profiles of the mixing paddles: (a) 90°, (b) forwarding, F, F60°, and (c) F30° offset.

50% relative humidity. Tensile testing was carried out employing a cross-head speed of 20 mm/min using BS 2782: Part 3, method 320A specimens. Non-standard specimens, with nominal dimensions $3.2 \times 63.5 \times 12.7\ mm^3$, were impact tested in Charpy configuration; BS 2782: Part 3, method 351A. Notches, with a tip radius of 0.25 mm, were cut using a Davenport, manual, broaching tool. The data for every test result reported herein are the mean values from tests on 10 specimens.

2.4. Characterisation

Bagley and Rabinowitsch corrected that the shear flow properties were determined using a Rosand capillary rheometer; the mean of two data points for each shear rate at 230 °C was determined. The thermal stabilities of the base resins were assessed through thermogravimetric analysis, by heating the sample at 20 °C min^{-1} in air from 50 to 750 °C. The oxidation temperature, T_{ox}, was determined from the point of initial deviation of the W versus T curve from a tangent drawn from $W = 100\%$, where W is the weight percentage of sample remaining at temperature, T. Flat surfaces of specimens taken from the extruded lace and the cores of the injection moulded tensile bars were prepared at −50 °C using an RMC ultramicrotome. Flat surfaces of specimens taken from the extruded lace and the cores of the injection moulded tensile bars were prepared at −50 °C using an RMC ultramicrotome. The flat surfaces were either etched with hot toluene, and coated with metal vapour, or stained with phosphotungstic acid and coated with carbon, before their image was captured with a scanning electron microscope (SEM). The SEM micrographs were digitised to form grey-scale images using a Primax D600 scanner. The number average dispersed phase diameters of selected objects in the images were determined from at least 200 particles for each specimen, calibrated with a graticule, using Imagepro image analysis software. For each selected object, the software measures the length of lines traversing the object that pass through the centre of gravity of the object at 5° intervals; the average of these lengths is reported as the average diameter. Typical micrographs used in these analyses are shown in Fig. 4. The number average particle diameter, D, was calculated $D = \sum n_i D_i / n$, where D_i and n_i are the average diameter and number of particles, i, respectively; n is the total number of particles. The number average particle diameters of the particles in the extrudates and moulded specimens were denoted as $D_{n(ext)}$ and $D_{n(m)}$, respectively. The amine end-group concentration of the pure PA6 and the blends were determined. The original PA6 resin (1.0000 g) was dissolved in a phenol/methanol mixture, containing 70 wt% phenol, whilst the PA6/iPP blends were dissolved in a two-phase solvent system comprising toluene and the phenol/methanol mixture at the reflux temperature under a nitrogen atmosphere. The solution was then cooled, five drops of thymol blue indicator (1%) were added, and the solution was titrated to the pink end-point with standardised HCl (0.0200 M); for the original PA6, the number average molecular weight, M_n, was calculated $M_n = 1000/[NH_2]_0$, where $[NH_2]_0$ is the concentration of amine end-groups.

3. Results and discussion

3.1. Description of the extrusion process

An estimate of the flow history was obtained through the following analysis. The capillary rheometer data showed that the melts of the constituent resins behaved approximately as power law fluids [15], i.e. $\tau = m\dot{\gamma}^n$ in the range $50 < \dot{\gamma} < 7000\ s^{-1}$. For iPP, $m = 11.2$ kPa s and $n = 0.33$, while for PA6, $m = 0.7$ kPa s and $n = 0.85$; $\dot{\gamma}$ is the corrected shear rate, n is the non-Newtonian exponent, m is the consistency, and τ is the corrected shear stress. Thus, the iPP exhibited more pronounced shear thinning than PA6 did; below $250\ s^{-1}$ iPP has the higher viscosity, whilst above this shear rate, PA6 has the higher viscosity. The viscosity ratio is unity at $250\ s^{-1}$. During twin-screw extrusion, the maximum shear rates were estimated from the expression [16]

$$\dot{\gamma} = \pi(D - 2h)N/h,$$

where D is the internal barrel diameter (16 mm), N is screw speed, and h is the distance between the tip of the mixing paddle and the wall of the barrel (0.2 mm). The calculated values were 408, 613, and 817 s^{-1} for screw speeds of 100, 150, and 200 min^{-1}, respectively. The minimum shear rates were estimated to be 15, 22, and 30 s^{-1} at screw speeds of 100, 150, and 200 min^{-1}, respectively, in the deepest part of the channel of the conveying sections where $h = 3.3$ mm. The shear rate in the die opening was estimated from [17]

$$\dot{\gamma} = (4Q_V/\pi r^3)(3n + 1/4n),$$

where $n = \mathrm{d}\log\tau/\mathrm{d}\log\dot{\gamma}$, and $Q_V = V_{T,P}m/t$; Q_V is the volumetric melt output rate, $V_{T,P}$ is the specific volume of the melt at temperature, T, and pressure, P, r is the radius of the die orifice (1 mm), m/t is gravimetric output rate, m is mass, and t is time. Thus, the shear rate through the circular-section die was around $90\ s^{-1}$. From the previous work [18], it was found that the phase inversion point estimated from $\phi_{inv} = [\eta_{PA}(1 - \phi_{inv})]/\eta_{PP}$ [19] using flow data determined at shear rates less than $90\ s^{-1}$ correlated with the observed morphology, where ϕ_{inv} is the volume fraction of polyamide at the phase inversion point and η_j is the viscosity of component j. For example, at a shear rate of $38\ s^{-1}$, the predicted phase inversion point was 34 vol% of PA6; the observed co-continuous range was from 30 to 40 vol% PA6. Thus, in the blends containing 40 vol% of iPP described herein, PA6 was the continuous phase in all of the extruded samples. The total power consumption during compounding, W_T, was analysed using the following

expression [13]

$$W_T = \sum((C_{P(j)}\Delta T) + \Delta H_{f(j)})Q_g w_{f(j)},$$

where $\Delta T = T_m - T_r$, T_m is the melt discharge temperature, T_r is room temperature, Q_g is the gravimetric output rate, $C_{P(j)}$ is the specific heat capacity, $\Delta H_{f(j)}$ is the heat of fusion, and $w_{f(j)}$ is the weight fraction of component j. The power input from mechanical work, W_M, was $W_M = S^*_e Q_g$. S^*_e is the corrected specific mechanical energy input from

$$S^*_e = ((T - T_0)/T_{max})(N/N_{max})P_{max}Q_g^{-1},$$

where T is the measured torque on the screws, T_0 is the torque necessary to turn the extruder when the barrel is empty, T_{max} is the maximum torque on the screws (24 N m), N_{max} is the maximum screw speed (300 min^{-1}), and P_{max} is the maximum power of the motor (750 W). The percentage of the total power, P_M, due to mechanical work causing a temperature rise of ΔT is $P_M = (W_M/W_T)100$. P_M is plotted versus S^*_e in Fig. 3. Between 10 and 50% of the power causing the temperature rise is derived from mechanical work. The extruder used in this work is one of the smallest in production and consequently has a relatively large surface area to free volume ratio, i.e. 0.47 $m^2 l^{-1}$. This compares with the values of 0.31 and 0.16 for 24 and 48 mm extruders, respectively, with the same centre line/radius ratio of 1.563, where centre line distance is the distance between the centres of the two screws. The fraction of heat generated through mechanical work may be expected to be greater in these larger machines due to the smaller surface area available for heat exchange between the melt and the barrel.

Sundararaj et al. [20] reported that the cooling time after melt processing may affect the observed morphology, due to coalescence in the quiescent melt before solidification was complete. Thus, the solidification time should be defined.

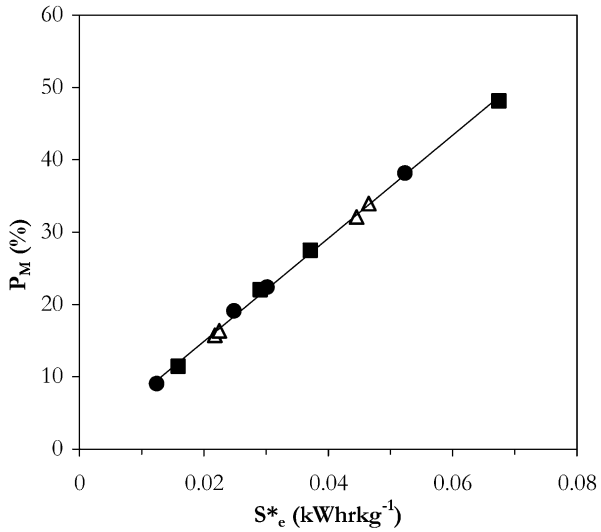

Fig. 3. Fraction of the total power derived from mechanical work, P_M used to increase the stock temperature by ΔT for samples containing (•) 1.0, (△) 2.4, and (■) 3.8 vol% of mPP.

The cooling rate of the extrudate was estimated using the Fourier equation [21]:

$$\partial T/\partial t = \alpha(\partial^2 T/\partial x^2),$$

where T is the temperature, t is time, α is the thermal diffusivity, and x is the distance between the centre of the cylindrical extrudate, from where the average dispersed phase diameters, $D_{n(ext)}$ were determined, and its surface that was in contact with the cooling water. The thermal diffusivity is determined from $\alpha = \kappa/\rho C_P$; κ is the specific thermal conductivity, ρ is the density, and C_P is the specific heat capacity. Relevant data are given in Table 1. It was assumed that α was constant over the temperature change. The dimensionless Fourier parameter, F_0, is calculated $F_0 = \alpha t/x^2$; x was half the extrudate thickness ($x = 3$ mm/2) for bi-directional heat transfer. A plot of the temperature gradient, $\Delta T = (T_{x,t} - T_w)/(T_0 - T_w)$, against F_0 for a cylinder was used to find F_0 at ΔT, and hence the time to reach $T_{x,t}$ was found [22]. T_w is the temperature of the cooling water (30 °C), T_0 is the initial melt temperature (typically 240 °C), $T_{x,t}$ is the temperature at x after time t. $T_{x,t}$ was taken as the estimated temperature where the crystal growth rate of polyamide was a maximum. This is at 180 °C, 40 °C below the melting point of 220 °C, 150 μm min^{-1} [23]. Thus, $T_{x,t} = 180$ °C, and hence for a melt temperature of 240 °C $F_0 = 0.17$ and the time taken to reach 180 °C is 3.8 s in the core of the extrudate. The crystallisation process in the core was assumed zeroth order three-dimensional spherulite growth. The number of spherulite nuclei in the volume of the core, N_V, is not known accurately in these samples, but the order of magnitude is estimated from previous work [24] as 2×10^{-3} μm^{-3}. To reach a maximum random packing fraction [25] of spherulites, ϕ_{max}, of $\phi_{max} \approx 0.7$, from

$$\phi_{max} = N_V \pi D_{nV}^3/6$$

at a spherulite growth rate of $dr_V/dt = 2.5$ μm s^{-1} [23], where r_V is the spherulite radius, the time taken, t_c, was 1.7 s after 180 °C was reached. The time taken for the melt to solidify and to freeze-in the melt-state morphology, t_s, was thus $t_s = t_c + t$, i.e. $t_s = 5.5$ s.

3.2. In situ formed compatibiliser

It has been reported that mPP reacts with amine end-groups of PA6 to form block copolymers [26]. In a recent study of a series of mPP/PA6/iPP blends [27], a semi-empirical model was established that related the mole fraction of amine end-groups reacted during twin-screw extrusion, f_r, to the mole ratio, χ_r, of the quantity of anhydride groups in the blend, χ_A, to the quantity of amine groups in the blend, χ_{NH_2}, and to the volume fraction of polyolefin, ϕ_{PO}, in the blend

$$f_r = k\chi_r^a/\phi_{PO},$$

Table 3
Estimated characteristics of the mPP/PA in situ reaction

Formulation #	ϕ_{mPP} (vol%)	χ_r	χ_A/χ_{NH_2}	$f_{r(max)}$ (mol%)	f_r^* (mol%)	ϕ_{bPA} (vol%)	ϕ_c (vol%)
1, 2, 3, and 4	1.0[a]	0.012[b]	1:83	1.2[c]	2.3[d]	1.4[e]	2.3[f]
9, 10, 11, and 12	2.4	0.029	1:34	2.9	4.3	2.6	5.0
5, 6, 7, and 8	3.8	0.047	1:21	4.7	6.0	3.5	7.3

[a] ϕ_{mPP} is the volume fraction of mPP in formulation #.
[b] Mole ratio $\chi_r = \chi_A/\chi_{NH_2}$, where $\chi_A = w_{mPP}[A]_0$, $\chi_{NH_2} = w_{PA}[NH_2]_0$, A is anhydride, and NH_2 is PA end-group.
[c] $f_{r(max)}$ is the maximum extent of amine reaction if 100% of the available anhydride groups react with end-groups.
[d] f_r^* is the mole fraction of amine end-groups reacted, calculated from the experimental model $f_r^* = k\chi_r^a/\phi_{PO}$.
[e] ϕ_{bPA} is the quantity of PA in the mPP-*b*-PA expressed as the percentage of the total sample volume $\phi_{bPA} = f_r^*\phi_{PA}$.
[f] ϕ_c is the quantity of in situ formed mPP-*b*-PA from $\phi_c = \phi_{mPP} + \phi_{bPA}$; only the final reported values were rounded.

where $\chi_r = \chi_A/\chi_{NH_2}$, $\chi_A = w_{mPP}[A]_0$, $\chi_{NH_2} = w_{PA}[NH_2]_0$, $f_r = ([NH_2]_b - [NH_2]_r)/[NH_2]_b$, $\phi_{PO} = \phi_{PP} + \phi_{mPP}$, w_{mPP} is the weight of mPP, w_{PA} is the weight of PA, $[A]_0$ is the molar concentration of anhydride groups in the mPP, $[NH_2]_0$ is the amine end-group concentration in the original PA, $[NH_2]_b$ is the amine end-group concentration in the PA determined from the PA/iPP blend processed in the absence of mPP, $[NH_2]_r$ is the residual amine end-group concentration in the blend processed in the presence of mPP, k is an dimensionless proportionality constant, and a describes the non-linearity of the relationship. It was found that $k = 0.2338$ and $a = 0.7336$ from the unweighted least sum-of-squares method [28] for the fit of the f_r values experimentally determined through titration [27] upon the model containing w_{mPP}, w_{PA}, $[A]_0$, $[NH_2]_0$, and ϕ_{PO} as independent variables, from

$$ss_{min} = \sum_{j=1}^{n} \Delta y_j^2,$$

where ss_{min} is the minimum sum of squares of n residuals, Δy, $\Delta y_j = f_{rj} - f_{rj}^*, f_{rj}$ is the experimental value, and f_{rj}^* is the corresponding value calculated from the model for datum j. The Solver program in the Microsoft Excel'97 spreadsheet software was used to accomplish this task [29]. Correlation of f_r with f_r^* yielded a correlation coefficient, r, of 0.997; r^2 showed that 99.4% of the variation in f_r was described by the model. In the ideal case, when 100% of the total available anhydride functional groups react with amine end-groups, the minimum concentration of residual end-groups, $[NH_2]_{r(min)}$, may be calculated:

$$[NH_2]_{r(min)} = [NH_2]_b - \left(\frac{w_{mPP}}{w_{PA}}[A]_0\right),$$

and hence the maximum mole fraction of end-groups that may react, $f_{r(max)}$, may be determined, i.e.

$$f_{r(max)} = ([NH_2]_b - [NH_2]_{r(min)})/[NH_2]_b.$$

The results for the three mPP contents used in this work are listed in Table 3. Apparently, the calculated values are slightly higher than the theoretical maximum values. The precision of the data used in the regression model was assessed from six replicate analyses [27]: %CV = 10%, where %CV = $(\bar{\sigma}/\bar{x})100$ is the coefficient of variation, $\bar{\sigma}$ is the sample standard deviation, and $\bar{x}$ is the arithmetic mean. The discrepancy between predicted and calculated is not significant in comparison with the experimental error. This relatively high level variation is thought to be due, in part, to the occlusion of some of the PA6 phase within the iPP domains thereby hampering the dissolution of the sample prior to titration. This was inferred from the micrographs of the stained specimens in Fig. 4(c) and (d) in which small light areas are seen within the dark iPP domains due to the presence of stained PA6. Orr et al. [30] determined that in a model study using miscible blends of amine end functionalised polystyrene (PS) with anhydride terminated PS that complete reaction was complete in less than 30 s at 180 °C and that this process was not controlled by chain end diffusion. Immiscible blends of anhydride end functional polyisoprene with amine end functional PS were found to react at rates that were influenced by the dilution of the reaction system; when the content of functionalised PS was greater than 10%, the reaction was essentially completed by around 120 s. In this work, given that there is an excess of the quantity of amine end-groups over the quantity of anhydride groups, ranging from 21:1 to 83:1 for compatibiliser contents of 3.8 and 1.0 vol%, respectively, it is reasonable to conclude that a large fraction of the available anhydride groups react with amine groups. Thus, the volume fraction of PA6 in the in situ formed copolymer, ϕ_{bPA}, is $\phi_{bPA} = f_r\phi_{PA}$ and the total volume fraction of compatibiliser, ϕ_c, is estimated: $\phi_c = \phi_{mPP} + \phi_{bPA}$.

A description of the molecular dimensions of the in situ formed compatibiliser in this work was obtained through the following reasoning. The molecular weight of the mPP was 97 500 g mol^{-1} [4]; the concentration of anhydride functional groups, $[A]$, was 45.9 μmol g^{-1} [31]. The average number of anhydride groups per iPP chain, f, is thus given by $f = [A]_0 M_w$, i.e. $f = 4.5$. The PA6 is assumed to have one amine end-group per molecule, i.e. $f = 1$, and given that between ≈2 and 6 mol% of these amine groups react with anhydride-groups, the in situ formed compatibiliser may comprise predominantly di- or tri-block species. No domains with micellar dimensions [32], $D_n \approx 0.1$ μm, were observed in the specimens described herein; micelles have been suggested to result from the in situ formation of

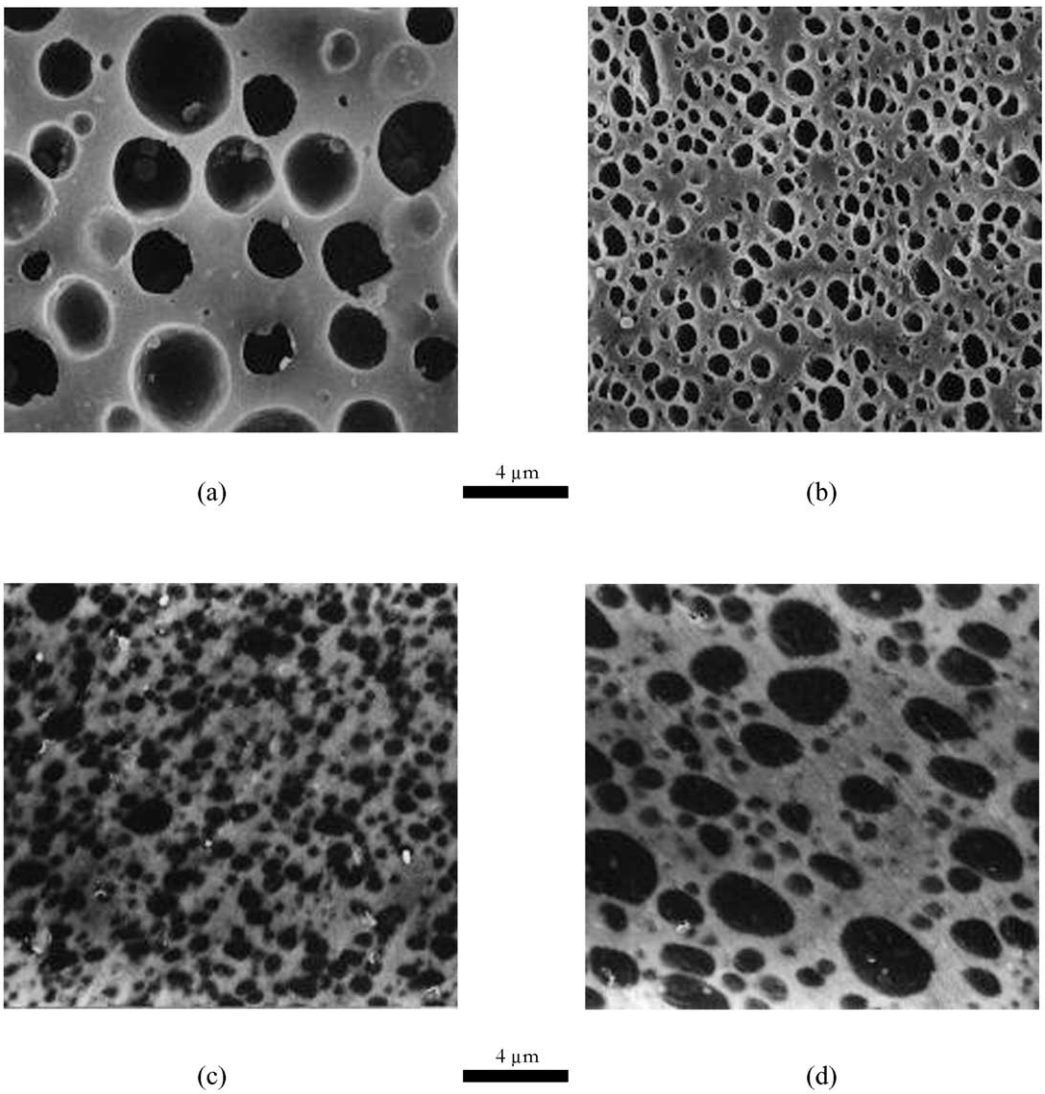

Fig. 4. Typical micrographs of the extrudate cores: dispersed iPP domains etched with toluene from (a) run #1 and (b) run #7; phosphotungstic acid stained samples from (c) run #6 and (d) run #11 (the PA6 continuous phase appears as the lighter gray shade after staining).

multi-block species [3]. The statistical segment length, b, of isotactic polypropylene in the melt-state at 200 °C is given by [33]

$$b = R_g M_w^{1/2},$$

where $b = 34$ pm mol$^{1/2}$ g$^{-1/2}$, and hence assuming that $(\partial b/\partial T)_P = 0$, $R_g = 12.9$ nm. The characteristic ratio, C_∞, for PA6 under theta conditions is 6.35 [34]. The statistical segment length is defined

$$b = (C_\infty n L^2/n_s)^{1/2},$$

where n is the number of backbone bonds, L is the mean bond length, $L = \sum n_i L_i/n$, in the PA6 backbone, assuming that $L_{C-C} = 154$ pm, $L_{CO-N} = 133.5$ pm, and $L_{NH-CR} = 145.5$ pm, $L = 150$ nm [35], and n_s is the number of statistical segments, in this case the number of repeat units:

$$R_g = b(n_s/6)^{1/2}.$$

Hence, $R_g = 6.0$ nm if $(\partial b/\partial T)_P = 0$. Thus, the reaction of one amine end-group with one anhydride functional group of the compatibiliser would result in the formation of a block copolymer with the coil size of the PA6 block around half the size of the iPP block. The sum of the radii of gyration of the PA6 and iPP block is 18.9 nm.

3.3. Dispersive mixing during extrusion

Fig. 4 shows typical micrographs of the etched and stained extrudate specimens. Fig. 5 is a plot of mean dispersed phase diameter in the core regions of the extruded blends, $D_{n(ext)}$, versus the total specific mechanical energy, S_e, from

$$S_e = (T/T_{max})(N/N_{max})P_{max}Q_g^{-1}.$$

For the blends with the lowest compatibiliser content, the larger dispersed domains were found for the lowest and

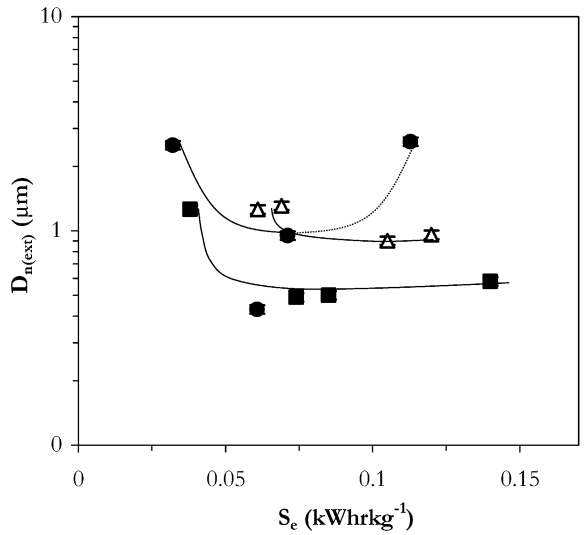

Fig. 5. Mean dispersed phase diameters in the extrudates, $D_{n(ext)}$, versus specific mechanical energy during compounding, S_e, for samples containing (•) 1.0, (△) 2.4, and (■) 3.8 vol% of mPP; the percentage coefficient of variation for the centre point samples #10 and #12 was 4.6%. $D_{n(ext)}$ was 7.2 μm for the uncompatibilised sample.

highest mixing energies; a minimum particle size was obtained at around 0.07 kW h kg^{-1}. The observation of larger droplets in unstable dispersions at higher mixing energies has been reported in the literature [36]. It was explained that the greater frequency of particle collisions and higher melt temperatures were the causes. Sundararaj and Macosko [9] commented that larger particles might result from the escape of particles without being broken because of the limited residence time in the extruder. Additionally, Roland and Bohm [37] showed that increasing shear rates increased the amount of coalescence. For the two highest mPP contents, a minimum particle size is reached at mixing energies of around 0.07 kW h kg^{-1}; domain size is largely independent of mixing energies greater than 0.07 kW h kg^{-1} for these samples. Mixing has been related to the interfacial tension coefficient, $\Gamma_{1,2}$, the radius of the dispersed phase particles, r_V, the viscosity of the matrix phase, η_m, and the shear rate in the form of the capillary number, C_a [38]:

$$C_a = \dot{\gamma} r_V \eta_m / \Gamma_{1,2}.$$

In this expression, the stress generated under flow in the blend is determined only by the stress generated in the pure matrix, i.e. $\tau = \dot{\gamma}\eta_m$ at a given shear rate. No account is made for interfacial slip, telescopic flow, or the influence of two-phase morphology upon viscosity [39]. Thus, the $\dot{\gamma}\eta$ term may be replaced by the average stress measured during compounding, τ_e, to give $C_a = \tau_e r_V / \Gamma_{1,2}$, and hence the observed mean domain diameter, D, after compounding is given $D^{-1} = f(C_a)$, where f denotes 'a function of'. The corrected specific mechanical energy may be used to calculate the average stress if the output rate has units of m^3 s^{-1} and the motor power is in Watts (W), i.e. $S_e^* = \tau_e =$ $_e^* = \tau_e =$ W m^{-3} s^{-1} = N m s^{-1} m^3 s^{-1} = N m^{-2} = Pa. Thus, $D = f(\tau_e^{-1})$ or $D = f(S_e^{-1})$. The observed dispersed phase dimensions are the result of the balance of interfacial and viscoelastic forces [40]. The total interfacial energy is the product of the interfacial tension coefficient and the interfacial area between the iPP and PA6 phases. The interface may be described by the specific interfacial area in the extrudate, S_{ext}. S_{ext} is related to the number average diameter in the cross-section, D_n, and the volume fraction of the dispersed domains, ϕ_d, through the following expressions [41]

$$\phi_d = V_d / \sum V_j, \qquad V_d = V_{PP} + V_{mPP}, \quad V_d = 4\pi n r_V^3/3,$$

$$D_V = 4D_n/\pi, \quad r_V = D_V/2,$$

and hence

$$S_{ext} = 4\pi n r_V^2,$$

assuming that the dispersed domains are spheres of uniform size, where r_V is the radius in volume of the domains, n is the number of domains per unit volume, $\sum V_j$, V_d is the total volume of the dispersed phase, and V_{iPP} and V_{mPP} are the volume of iPP and mPP in the sample, respectively. For example, if $D_n = 0.5$ μm and $\phi_d = 0.4$, then $S_{ext} = 4.8$ μ_m^{-1}. The data from Fig. 5 were re-plotted in the form of the ratio of the interfacial area divided by the volume fraction of copolymer in the blend, S_{ext}/ϕ_c, versus τ_e in Fig. 6. For the lowest compatibiliser content, the ratio varies by a relatively large amount with τ_e in comparison with the values for the compounds containing 2.4 and 3.8 vol% of mPP that reach a limit at approximately $S_{ext}/\phi_c \approx 45$ μm^{-1} for average stresses greater than 100 MPa. It may be inferred that the dispersive mixing was largely controlled by the ratio of compatibiliser content to interfacial area generated at mixing stresses higher than a critical value.

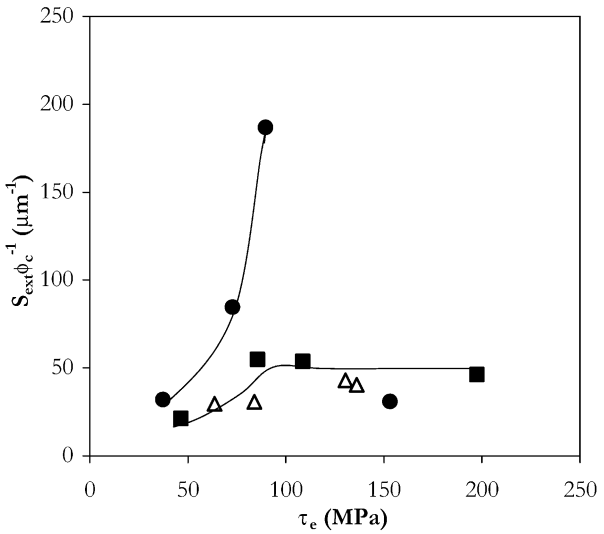

Fig. 6. Ratio of specific interfacial area to volume fraction, at 25 °C, of in situ compatibiliser, $S\phi_c^{-1}$, versus average stress during extrusion, τ_e, for samples containing (•) 1.0, (△) 2.4, and (■) 3.8 vol% of mPP.

As will be discussed in Section 3.4, the particles present in the 1.0 vol% mPP compounds were the least stable during moulding, possibly because of the high ratio of interfacial area to compatibiliser content. If the in situ formed compatibiliser were located predominantly at the iPP/PA6 interfaces, the average thickness of the compatibiliser layer, λ_c, could be estimated: $\lambda_c = \phi_c/S_{ext}$. For the samples with $\phi_{mPP} = 2.4$ or 3.8 vol%, λ_c reaches a limiting value of $\approx$23 nm for average stresses greater than 100 MPa. Thus, the estimated average thickness is of comparable size to the sum of the estimated radii of gyration of the iPP and PA6 blocks, i.e. $\approx$19 nm. This value may not be directly comparable with the interfacial thickness data published in other work [5], since it is not certain which material in the in situ formed compatibiliser contributes to the interphase that is measured experimentally. The constancy of the ratio S_{ext}/ϕ_c at higher mixing stresses may correspond to the limiting effect of the in situ formed mPP-*b*-PA6. The production of smaller particles would result in the generation of fresh interface. This would be achieved only by doing work against the relatively high interfacial tension of the 'bare' PA6/iPP interface. Experimental values for the PA6/iPP interfacial tension range from 7.8 mN m^{-1} at 250 °C [7] to 12.5 mN m^{-1} at 225 °C [6]. Since there may be insufficient compatibiliser present to stabilise the newly created interface, coalescence may take place rapidly, resulting in the constancy of the S_{ext}/ϕ_c ratio for the higher compatibiliser contents. Favis [42] studied the relationship between interfacial area generation and compatibiliser content, under a single melt processing condition in polyolefin/blends. It was observed that a limiting interfacial area was reached that was inferred to indicate saturation of the interface with in situ formed compatibiliser. Sundararaj and Macosko [9] showed that in situ reaction during polymer blending suppressed domain coalescence through stabilising the interface resulting in smaller particles and narrower particle size distributions. The principal effect was not the enhancement of dispersion due to a reduction of interfacial tension.

3.4. The moulding process

The power dissipated per unit volume during plasticisation, p, in the injection moulder was taken as [43]

$$p = \eta(\dot{\gamma}_c)^2,$$

where η is the steady shear viscosity at shear rate, $\dot{\gamma}_c$, in the channel of the screw in the metering zone [16]; for the injection moulder D, the internal barrel diameter, was 24 mm; N, the screw speed, was 100 min^{-1}; h, the screw channel depth, was 2 mm. Thus, $\dot{\gamma}_c = 52$ s^{-1}. Specific mechanical energy input during plasticisation, S_p, was calculated $S_p = pt_p$, where t_p is the plasticisation time (5 s); $S_p = 7.5$ MJ m^{-3} at 230 °C. The shear rate in the nozzle, $\dot{\gamma}_N$, was estimated from the same method used to estimate the shear rate in the extruder die. In this case, $Q = V_{T,P}m/t_I$, where Q is the melt injection rate, m the shot weight (15 g), $V_{T,P}$ is the specific volume of the melt at temperature, T, and injection pressure, P (3.4 MPa), t_I is the injection time (2 s), and r is the radius of the nozzle orifice (1.25 mm): $\dot{\gamma}_N = 6788$ s^{-1}, for an average specific melt volume of 1.19 cm^3 g^{-1} for melts at 230 °C under 32.4 MPa of pressure [14]. Cooling of the moulding was described by the Fourier equation solved for the bi-directional heat transfer from a flat sheet [21]. In this case, x is half the moulding thickness, i.e. 3.2 mm/2, $\Delta T = 0.71$, $F_0 = 0.25$, and hence $t = 6.4$ s. The solidification time is the sum of the cooling and crystallisation times, i.e. 8.1 s. The average domain diameters in the cross-section of the cores of injection moulded tensile bars, $D_{n(m)}$, are plotted as a function of the mixing energy during extrusion, S_e, in Fig. 7. The stability of the iPP dispersion produced in the extruder during injection moulding was quantified through the difference, ΔD_n, in the average domain diameter of extrudate and $D_{n(m)}$:

$$\Delta D_n = |D_{n(ext)} - D_{n(m)}|.$$

The plot in Fig. 8 shows the relationship between ΔD_n and the original particle diameter in the extrudate, $D_{n(ext)}$. It can be seen that the larger particles in the extrudate undergo the largest changes in dimension during injection moulding. Moreover, samples containing 1 and 0 vol% compatibiliser undergo the largest changes during injection moulding. Apparently the flow conditions in the injection moulder were sufficiently vigorous to change the domain dimensions of particles of mean diameter of 1 μm and larger, both through dispersion and coalescence. The smallest fraction of particles with mean diameters around 0.5 μm, in the

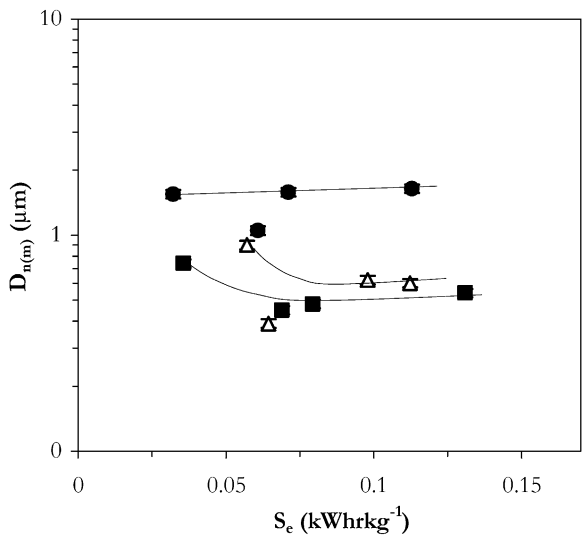

Fig. 7. Mean dispersed phase diameters in the cores of the injection moulded tensile bars, $D_{n(m)}$, versus specific mechanical energy during compounding, S_e, for samples containing (•) 1.0, (△) 2.4, and (■) 3.8 vol% of mPP; the percentage coefficient of variation for the centre point samples #10 and #12 was 2.3%. $D_{n(m)}$ was 13.4 μm for the uncompatibilised sample.

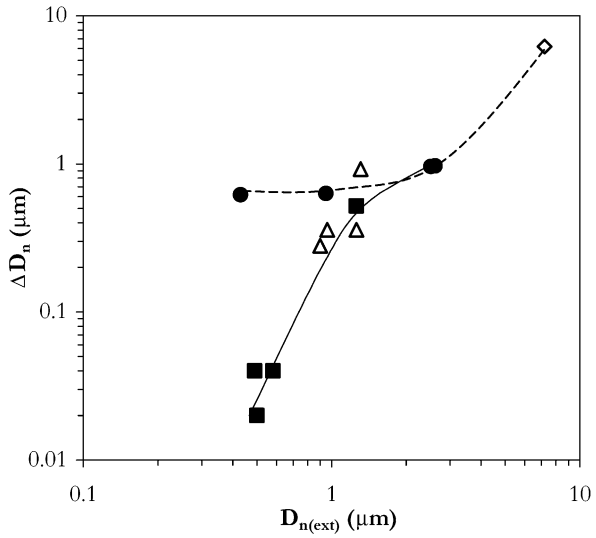

Fig. 8. Difference between the mean dispersed phase diameters in the extrudate and the mean diameters in the corresponding mouldings, $\Delta D_n = |D_{n(ext)} - D_{n(m)}|$, versus $D_{n(ext)}$, for samples containing (◇) 0, (•) 1.0, (△) 2.4, and (■) 3.8 vol% of mPP.

formulations containing 2.4 and 3.8 vol% of compatibiliser, were not greatly altered during injection moulding. Several samples containing 2.4 vol% of compatibiliser had mean domain sizes of 0.56 μm in the injection mouldings; after annealing under quiescent conditions at 230 °C for 10 min in an oil bath, the domain diameters increased to 0.68 μm. Thus, 2.4 vol% of compatibiliser was sufficient to largely stabilise the iPP dispersion.

Impact test data for all formulations are included in Table 1; the tensile breaking strains are plotted versus S_e during mixing in Fig. 9. Regression analysis of the mechanical test results upon the compatibiliser content,

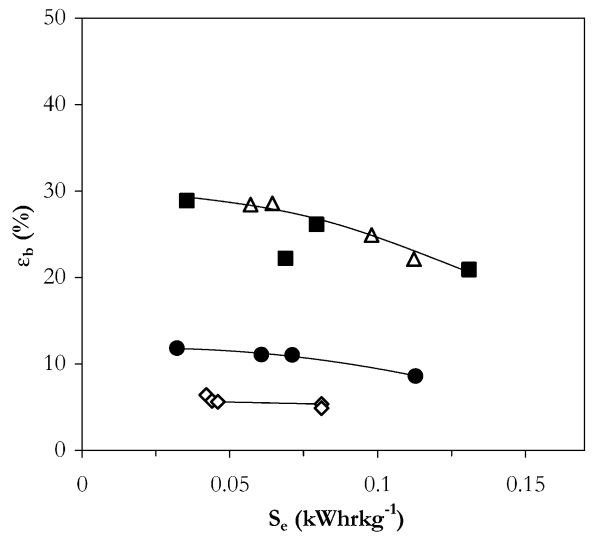

Fig. 9. Plot of tensile breaking strain, ε_b, versus specific mechanical energy input, S_e, for samples containing (◇) 0, (•) 1.0, (△) 2.4, and (■) 3.8 vol% of mPP; the percentage coefficient of variation for the centre point samples was 8.4%. For the original PA6, $\varepsilon_b = 11.4\%$ and for the original iPP, $\varepsilon_b > 345\%$.

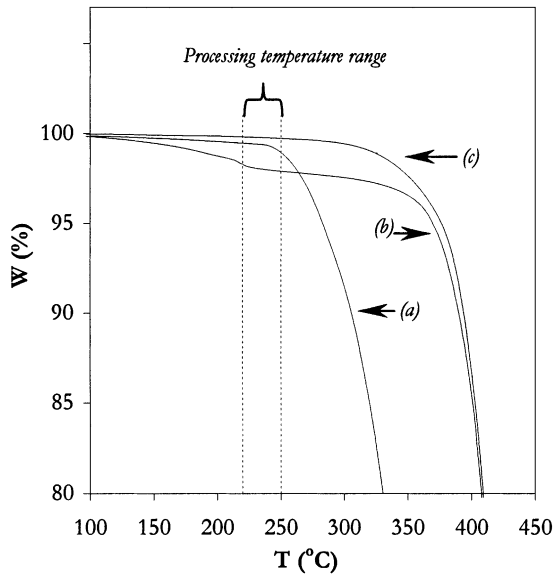

Fig. 10. TGA traces for (a) mPP, (b) PA6, and (c) iPP heated in air; T_{ox} was 255, 355, and 338 °C, respectively.

screw configuration, and screw speed revealed that compatibiliser was the most important factor affecting the mechanical properties. Strain at break decreased with increasing mechanical energy input for all compatibiliser contents and was independent of domain particle size when the compatibiliser content was 2.4 and 3.8 vol%. Fig. 10 shows TGA traces for the original PA6, iPP, and mPP resins; the corresponding T_{ox} values were 355, 338, and 255 °C, respectively. The decrease in breaking strain may be related to the degradation during compounding under the higher mixing energies, particularly of the compatibiliser, T_{ox} of which is close to the processing temperature range. Moreover, amine end-group titration of the uncompatibilised blend after compounding showed that there was an increase in the number of end-groups of the PA from 49.1 μmol g^{-1}, in the as-supplied PA6, to 51.6 μmol g^{-1} in the processed sample suggesting some degradation of the PA6 phase. Yield stress, initial tangent modulus, and notched Charpy impact energy were insensitive to mixing energy input over the range studied.

4. Conclusions

Specific energy was found a useful single parameter to describe the observed morphologies in the extruded samples and injection mouldings. Specific energy inputs of 0.07 kW h kg^{-1} were sufficient to reach the limiting values of the mean dispersed particle diameters at a given compatibiliser content. The coarser and less stable dispersions produced in the twin-screw extruder underwent the greatest changes in dimension during injection moulding. No correlation was found between the domain size and ductility of the blends. The latter property was only affected by the compatibiliser content and the mechanical energy

input. The greatest ductility was found for the lowest energy inputs, regardless of dispersed phase particle size.

Acknowledgments

The authors would like to thank MTEC for their financial support of this work and for use of the TGA. Thanks also go to Chemical Innovation, Co. Ltd, Thailand, for donation of the compatibiliser.

References

[1] Abdellah A, Utracki LA. Prog Rubber Plast Technol 1997;13(3):153.
[2] Marechal P, Coppens G, Legras R, Dekoninck JM. J Polym Sci, Part A: Polym Chem 1995;33:757.
[3] Gonzalez-Montiel A, Keskkula H, Paul DR. J Polym Sci, Part B: Polym Phys 1995;33:1751.
[4] Majumbar B, Keskkula H, Paul DR. Polymer 1994;35(7):1386.
[5] Li H, Chiba T, Higashida N, Yang Y, Inoue T. Polymer 1997;38(15): 3921.
[6] Jannerfeldt G, Boogh L, Manson JAE. J Polym Sci, Part B: Polym Phys 1999;37:2069.
[7] Kirjava J, Rundqvist T, Holsti-Miettinen R, Heino M, Vainio T. J Appl Polym Sci 1995;55:1069.
[8] Asthana H, Jayaraman K. Macromolecules 1999;32:3412.
[9] Sundararaj U, Macosko CW. Macromolecules 1995;28:2647.
[10] Progelhof RC, Throne JL. Polymer fluid and chemical properties. Polymer engineering principles. Munich: Hanser; 1993. p. 337, Chapter 4.
[11] Michaeli W. Properties of polymeric melts. Extrusion dies for plastics and rubber, 2nd rev. ed. Munich: Hanser; 1992. p. 44, Chapter 2.
[12] Michaeli W. Properties of polymeric melts. Extrusion dies for plastics and rubber, 2nd rev. ed. Munich: Hanser; 1992. p. 45, Chapter 2.
[13] Morton-Jones D. Polymer processing, 1st ed. London: Chapman & Hall; 1989.
[14] Grulke EA. Polymer processing. Polymer process engineering, 1st ed. New Jersey: PTR Prentice-Hall; 1994. p. 577, Chapter 10.
[15] Rauwendaal C. Important polymer properties. Polymer extrusion, 2nd ed. Munich: Hanser; 1990. p. 182, Chapter 6.
[16] Rauwendaal C. Important polymer properties. Polymer extrusion, 2nd ed. Munich: Hanser; 1990. p. 181, Chapter 6.
[17] Nielson LE. Instruments. Polymer rheology, 1st ed. New York: Marcel Dekker; 1977. p. 16, Chapter 2.
[18] Kaihirun M. The effect of filler upon the phase morphology and properties of polypropylene/polyamide 6 blends. MSc Thesis. Department of Chemistry, Mahidol University, Thailand; 1999. ISBN 974-662-927-1.
[19] Jordhamo GM, Manson JA, Sperling LH. Polym Engng Sci 1986;26: 517.
[20] Sundararaj U, Macosko CW, Nakayama A, Inoue T. Polym Engng Sci 1995;35:100.
[21] Crawford RJ. Analysis of flow during processing. Plastics engineering, 2nd ed. Oxford: Pergamon Press; 1987. p. 279, Chapter 5.
[22] Crawford RJ. Analysis of flow during processing. Plastics engineering, 2nd ed. Oxford: Pergamon Press; 1987. p. 280, Chapter 5.
[23] Progelhof RC, Throne JL. Polymer fluid and chemical properties. Polymer engineering principles. Munich: Hanser; 1993. p. 129, Chapter 2.
[24] Parchana B. Flow induced phase morphologies in partially miscible polyolefin blends. MSc Thesis. Department of Chemistry, Mahidol University, Thailand; 2000.
[25] Wypych G. Dispersion, morphology, and system rheology. Fillers. Canada: Chemtec Publishing; 1993. p. 143, Chapter 4.
[26] Xanthos M, Dagli SS. Polym Engng Sci 1991;31(13):929.
[27] Tangchareetsakull P. Analysis of the reactive processing of twin-screw extruded polyamide-6/polyolefin blends. MSc Thesis. Department of Chemistry, Mahidol University, Thailand; 2001.
[28] Moore DS, McCabe GP. Looking at data: relationships. Introduction to the practice of statistics, 1st ed. New York: Freeman and Company; 1989. p. 175, Chapter 3.
[29] Harris DC. J Chem Ed 1998;75(1):119.
[30] Orr CA, Bates FS, Macosko CW. Creating block copolymers via melt coupling reactions. Proceedings of the Polymer Processing Society, December 1–3. Bangkok, Thailand: Asia/Australia Regional Meeting; 1999. p. 1.
[31] [31] Dupont Co. Ltd. Fusabond 109D suppliers specification, 1997.
[32] Gleinser W, Braun H, Friedrich C, Cantow HJ. Polymer 1994;35(1): 128.
[33] Ballard DGH, Cheshire P, Longman G, Schelten J. Polymer 1978;19: 379.
[34] Bicerano J. Properties of polymers in dilute solution. Prediction of polymer properties, 1st ed. New York: Marcel Dekker; 1993. p. 286, Chapter 12.
[35] Atkins PW. The structures and properties of macromolecules. Physical chemistry, 3rd ed reprint. Oxford: Oxford University Press; 1987. p. 625, Chapter 25.
[36] Curry JE. Practical aspects of processing of blends. In: Folkes MJ, Hope PS, editors. Polymer blends and alloys, 1st ed. London: Blackie Academic and Professional; 1993. p. 39. Chapter 2.
[37] Roland CM, Bohm GGA. J Polym Sci, Part B: Polym Phys 1984;22: 79.
[38] Elmendorp JJ. Dispersive mixing in liquid systems. In: Rauwendaal C, editor. Mixing in polymer processing, 1st ed. New York: Marcel Dekker; 1991. p. 30. Chapter 2.
[39] Utracki LA. Rheology of polymer alloys and blonds. Polymer blends and alloys: thermodynamics and rheology, 1st ed. Munich: Hanser; 1989. p. 178, Chapter 3.
[40] Wu S. Polym Engng Sci 1987;27:335.
[41] Dehoff RT. Measurement of number and average size in volume. Quantitative microscopy, 1st ed. New York: McGraw-Hill; 1968. p. 131, Chapter 5.
[42] Favis BD. Polym Commun 1994;35(7):1552.
[43] Morton-Jones DH. Mixing. Polymer processing, 1st ed. London: Chapman & Hall; 1989. p. 71.